Vacuum 186 (2021) 110057

Contents lists available at ScienceDirect

Vacuum

journal homepage: http://www.elsevier.com/locate/vacuum

Dense $Ti_{0.67}Hf_{0.33}B_{1.7}$ thin films grown by hybrid HfB_2-HiPIMS/TiB_2-DCMS co-sputtering without external heating

Babak Bakhit [a,*], Stanislav Mráz [b], Jun Lu [a], Johanna Rosen [a], Jochen M. Schneider [b], Lars Hultman [a], Ivan Petrov [a,c,d], Grzegorz Greczynski [a]

[a] Thin Film Physics Division, Department of Physics (IFM), Linköping University, Linköping, SE-58183, Sweden
[b] Materials Chemistry, RWTH Aachen University, Kopernikusstr. 10, Aachen, D-52074, Germany
[c] Materials Research Laboratory and Department of Materials Science, University of Illinois, Urbana, IL, 61801, USA
[d] Department of Materials Science and Engineering, National Taiwan University of Science and Technology, Taipei, 10607, Taiwan

ARTICLE INFO

Keywords:
Thin films
Borides
Low-temperature sputter deposition
Hybrid HiPIMS/DCMS
Hardness

ABSTRACT

There is a need for developing synthesis techniques that allow the growth of high-quality functional films at low substrate temperatures to minimize energy consumption and enable coating temperature-sensitive substrates. A typical shortcoming of conventional low-temperature growth strategies is insufficient atomic mobility, which leads to porous microstructures with impurity incorporation due to atmosphere exposure, and, in turn, poor mechanical properties. Here, we report the synthesis of dense $Ti_{0.67}Hf_{0.33}B_{1.7}$ thin films with a hardness of ~41.0 GPa grown without external heating (substrate temperature below ~100 °C) by hybrid high-power impulse and dc magnetron co-sputtering (HfB_2-HiPIMS/TiB_2-DCMS) in pure Ar on Al_2O_3(0001) substrates. A substrate bias potential of −300 V is synchronized to the target-ion-rich portion of each HiPIMS pulse. The limited atomic mobility inherent to such desired low-temperature deposition is compensated for by heavy-mass ion (Hf^+) irradiation promoting the growth of dense $Ti_{0.67}Hf_{0.33}B_{1.7}$.

1. Introduction

The technological desire for low-temperature techniques to grow dense and hard refractory thin films motivates scientific investigation [1–4]. Low-temperature growth offers a valuable reduction in energy consumption and allows coating temperature-sensitive substrates such as polymers and low-melting-point alloys based on, for example, Mg and Al. However, films grown without external heating typically exhibit open, under dense microstructures due to limited atomic mobility, which can adversely affect physical and mechanical properties [3,5]. For instance, the hardness of as-deposited TiN thin films grown by conventional dc magnetron sputtering (DCMS) without external heating (substrate temperature $T_s < 120$ °C) is ~8 GPa, which is considerably lower than that of similar layers deposited at 500 °C, with a bulk-like value of ~20 GPa [6].

One approach to increase the atomic mobility during the low-temperature growth is to irradiate the growing film surface with energetic ions [2,3]. In DCMS, gas ions are used to bombard the growing film surface by applying a negative continuous bias to the substrate. This results in an increased film density [1–3,7], but it also leads to the incorporation of gas atoms into the interstitial positions or gas bubble formation [8] and consequently, deterioration of film properties [9,10].

Our working hypothesis is that these drawbacks can be avoided during boride synthesis by replacing the gas-ion irradiation with film-forming metal ions. The latter cannot be achieved with DCMS as the ionization levels of sputter-ejected atoms are low [11]. However, in high-power impulse magnetron sputtering (HiPIMS), highly-ionized fluxes of sputtered target species are readily available [12]. This, together with the controllable time separation between metal- and gas-ion fluxes incident at the substrate that occurs due to severe gas rarefaction in front of the target [13,14], enables selective tuning of both energy and momentum of incident metal-ion fluxes [15]. If the mass of incident metal ions is sufficiently high, applying a negative substrate-bias pulse that is synchronized to the target-ion-rich portion of each HiPIMS pulse provides a recoil density and energy required to generate the mobility to eliminate under-dense regions forming during the low-temperature growth [5]. The validity of the heavy-mass-ion-synchronized HiPIMS/DCMS film growth technique

* Corresponding author.
E-mail address: babak.bakhit@liu.se (B. Bakhit).

https://doi.org/10.1016/j.vacuum.2021.110057
Received 27 November 2020; Received in revised form 28 December 2020; Accepted 6 January 2021
Available online 12 January 2021

was demonstrated in a reactive-gas sputtering mode by growing dense $Ti_{0.92}Ta_{0.08}N$ ($T_s < 120$ °C) [6] and $Ti_{0.40}Al_{0.27}W_{0.33}N$ ($T_s < 150$ °C) [16] as well as $Ti_{0.41}Al_{0.51}Ta_{0.08}N$ ($T_s < 150$ °C) [17].

Here, we demonstrate a related approach, however, in a non-reactive deposition mode and for compound TM diboride targets to grow $Ti_{0.67}Hf_{0.33}B_{1.7}$ thin films in a hybrid HfB_2-HiPIMS/TiB_2-DCMS co-sputtering scheme without external heating. TiB_2 is employed as a common TM diboride material system, while HfB_2 target operated in HiPIMS mode serves as a source of heavy mass ions. We choose this ternary diboride because it forms solid solutions (as also shown herein) and, thus, is a suitable system to study the effects of heavy-mass ion irradiation on film densification. The substrate temperature does not exceed 100 °C during the growth. The incident ion energy is controlled by applying a substrate bias of −300 V synchronized to the Hf^+-ion-rich portion of each HiPIMS pulse, while the deleterious role of gas ion irradiation is minimized by keeping the substrate at floating potential during the DCMS phase. Such energetic heavy-mass ion irradiation is used to demonstrate the low-temperature synthesis of dense $Ti_{0.67}Hf_{0.33}B_{1.7}$ films exhibiting a smooth surface and nanoindentation hardness exceeding 40 GPa.

2. Experimental

$Ti_{0.67}Hf_{0.33}B_{1.7}$ thin films are grown in a CC800/9 CemeCon AG sputtering system equipped with rectangular stoichiometric TiB_2 and HfB_2 targets (8.8 × 50 cm^2). Al_2O_3(0001) substrates (1.5 × 1.5 cm^2) are cleaned sequentially in acetone and isopropyl alcohol and then mounted symmetrically with respect to the targets, which are tilted toward the substrates, resulting in a 21° angle between the substrate normal and the normal to each target. The target-to-substrate distance is 20 cm, and the system base pressure is 3.0 × 10^{-6} Torr (0.4 mPa). The chamber is degassed before deposition in a two-step procedure. First, two resistive heaters are powered to 2000 W for 1 h, resulting in a chamber temperature of ~110 °C at the substrate position, i.e., high enough to promote water desorption necessary to reach the base pressure. Thereafter, the power applied to both heaters is switched off for 1 h such that the temperature drops to ~60 °C. The films are then deposited without external heating, resulting in T_s = ~100 °C toward the end of the 1600-s long deposition (due to plasma heating). The temperature is measured with a calibrated thermocouple bonded to a dummy substrate holder and placed next to the actual substrate. The Ar pressure during deposition is 3 mTorr (0.4 Pa). The targets are sequentially DCMS pre-sputtered in Ar at 2000 W for 60 s with closed cathode shutters prior to depositing the films.

$Ti_{0.67}Hf_{0.33}B_{1.7}$ films are grown using a hybrid target-power scheme (HfB_2-HiPIMS/TiB_2-DCMS), in which the TiB_2 target is continuously sputtered by DCMS at 2500 W, while the HfB_2 magnetron is operated in HiPIMS mode by applying an average target power of 2200 W, with 100-μs pulses and a pulsing frequency of 200 Hz. The peak HfB_2-target current density $J_{T,peak}$ is ~1.1 A/cm^2. After the initial stages of film growth necessary to form a continuous layer that provides electrical conductivity, a substrate bias of −300 V is synchronized with the 200-μs target-ion-rich portion of each HiPIMS pulse (4% duty cycle), as confirmed by time-resolved mass spectroscopy analysis (see Fig. 1). The substrate bias pulse begins at time t = 30 μs following the HiPIMS pulse initiation (t = 0 μs). The substrates are maintained at the floating potential of −10 V for the rest of the period.

In-situ time-resolved analyses of ion fluxes incident at the substrate plane during HiPIMS sputtering of HfB_2 target in Ar are performed with a Hiden Analytical EQP1000 instrument. The orifice of the spectrometer is placed at the substrate position facing the HfB_2 target. Data are recorded during 100 consecutive HiPIMS pulses such that the total acquisition time per data point is 1 ms. Additional details are given in reference [18]. The measured isotopes include $^{178}Hf^+$, $^{10}B^+$, and $^{36}Ar^+$, selected to avoid detector saturation. The data presented in Fig. 1 are scaled using isotope abundances to represent the actual ion concentrations in the plasma. A Tektronix 500 MHz digital oscilloscope is used to measure the current and voltage waveforms both at the cathode as well as at the substrate.

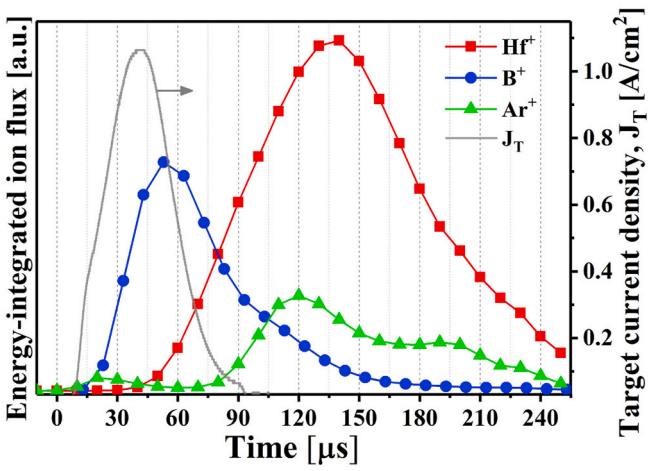

Fig. 1. Time evolution of energy-integrated Hf^+, B^+, and Ar^+ ion fluxes incident at the substrate plane during and after a 100-μs HfB_2-HiPIMS pulse, in which the HfB_2 target is sputtered at an average power of 2200 W. The continuous grey line, with no data symbols, is the HfB_2-target current density J_T as a function of time t. The peak HfB_2-target current density $J_{T,peak}$ is ~1.1 A/cm^2. A substrate bias V_s of −300 V is synchronized with the target-ion-rich portion of each pulse (from 30 to 230 μs after the HiPIMS pulse initiation). Data points correspond to the number of ions collected during the interval from (t-5) to (t+5) μs.

The film composition is obtained from time-of-flight elastic recoil detection analysis carried out in a tandem accelerator with a 36 MeV $^{127}I^{8+}$ probe beam incident at 67.5° with respect to the surface normal of sample. Recoils are detected at 45°. A Zeiss LEO 1550 scanning electron microscope (SEM) is used to obtain the film's thickness and cross-sectional morphology. A θ-2θ X-ray diffraction (XRD) scan is carried out using a PANalytical Empyrean diffractometer to determine crystal structure and orientation. Plan-view transmission electron microscopy (TEM) analyses are carried out in a monochromated and double-corrected FEI Titan^3 60–300 electron microscope operated at 300 kV. The TEM specimens are prepared by the focused ion beam method using a Carl Zeiss Cross-Beam 1540 EsB system.

Nanoindentation hardness and elastic modulus of the film are determined in an Ultra-Micro Indentation System equipped with a sharp Berkovich diamond tip calibrated using a fused-silica standard. For the hardness H and elastic modulus E measurements, the film is indented using a fixed load of 12 mN, while indention depths are maintained below 10% of the film thickness. The results are analyzed using the Oliver and Pharr method [19]. The E value is calculated from the reduced elastic modulus using the diamond indenter's elastic modulus (1141 GPa) and Poisson's ratio ν = 0.07. The ν value of $Ti_{1-x}Hf_xB_y$ is unknown, but estimated here based upon a linear interpolation between ν for TiB_2 (~0.11 [20]) and ν for HfB_2 (~0.16 [21]), which is ~0.13. The reported hardness and elastic modulus values are averages obtained from 40 indentations.

3. Results and discussion

Time-dependent intensities of energy-integrated Hf^+, B^+, and Ar^+ ion fluxes incident at the substrate plane during and after 100-μs HfB_2-HiPIMS pulses, with an average HfB_2-target power of 2200 W and peak current density $J_{T,peak}$ of ~1.1 A/cm^2, are plotted in Fig. 1. During the time when the synchronized −300-V substrate bias is applied, 30–230 μs following the HiPIMS pulse initiation, the B^+ ions are the first significant ion fraction reaching the substrate (from 30 to 80 μs), and then, the plasma is dominated by the Hf^+ ion flux (from 80 to 230 μs after the

HiPIMS pulse initiation). The time delay observed between the B^+ and Hf^+ ion fluxes irradiating the substrate position is mainly attributed to the longer time-of-flight of the Hf^+ ions, as Hf is significantly heavier than B ($m_{Hf} = 178.5$ amu and $m_B = 10.8$ amu) [22]. The pre-dominance of the Hf^+ ions is due to strong gas rarefaction and quenching of electron-energy distribution [23] since the first-ionization potential of Hf (6.8 eV [24]) is lower than the first-ionization potentials of B (8.3 eV [24]) and Ar (15.8 eV [24]) as well as the second-ionization potentials of Hf (14.9 eV [24]), B (25.2 eV [24]), and Ar (27.6 eV [24]). The Hf^{2+}/Hf^+ ratio during the 200-μs synchronized substrate bias is 0.078.

The hybrid HfB_2-HiPIMS/TiB_2-DCMS film growth results in the $Ti_{0.67}Hf_{0.33}B_{1.7}$ films. The total concentration of carbon, nitrogen, and oxygen is ~0.9 at%. The Ar concentration is ~1.0 at%. The high Ar concentration in the $Ti_{0.67}Hf_{0.33}B_{1.7}$ thin film is due to the overlap between the Ar^+ and Hf^+ ion fluxes in the time interval 90–230 μs, i.e., during the time when the substrate is biased at −300 V (cf. Fig. 1).

Fig. 2 presents cross-sectional and plan-view SEM images of $Ti_{0.67}Hf_{0.33}B_{1.7}$ thin film. The film has an average thickness of ~1100 nm. The cross-sectional SEM image, Fig. 2(a), exhibits that $Ti_{0.67}Hf_{0.33}B_{1.7}$ has a dense structure, while the plan-view SEM image in Fig. 2(b) indicates that the $Ti_{0.67}Hf_{0.33}B_{1.7}$ film has a smooth surface. The formation of the dense structure with such a smooth surface, which results in less impurity incorporation from atmosphere exposure, is attributed to the high atomic mobility induced during the low-temperature growth by bombarding the growing film with energetic heavy Hf^+ ions generated by HiPIMS sputtering of the HfB_2 target. Neutralized Ar ions backscattered from the HfB_2 target surface may also contribute to the film's densification; however, such contribution is much smaller compared to DCMS because Ar sputtering occurs for a short initial fraction of the HiPIMS pulse, before the transition to metal-dominated plasma. Intensive Ar rarefaction that takes place during the later phase is expected to further reduce the flux of backscattered neutrals [22]. Hence, the dominant densification effect is due mainly to the high-mass-ion irradiation. The negligible role of backscattered Ar neutrals in densification of DCMS-deposited layers is further supported by experiments involving Ta target (similar mass to Hf) to grow $Ti_{0.92}Ta_{0.08}N$ and $Ti_{0.41}Al_{0.51}Ta_{0.08}N$ films without external heating [6, 17]. Switching from Ta-HiPIMS to Ta-DCMS in the same target configuration resulted in a complete loss of densification effects.

The XRD θ-2θ scan from the $Ti_{0.67}Hf_{0.33}B_{1.7}$ thin film is shown in Fig. 3. Vertical solid and dashed lines correspond to reference powder-diffraction peak positions for TiB_2 [25] and HfB_2 [26], respectively. The peak at 41.7°, indicated with a diamond symbol, arises from the $Al_2O_3(0001)$ substrate. The other broad peaks appearing at 26.4° and 54.5° originate from the hexagonal AlB_2-type structure and correspond to (0001) and (0002) planes, respectively. The XRD result reveals that $Ti_{0.67}Hf_{0.33}B_{1.7}$ forms a solid solution with a highly preferred crystallographic orientation along the [0001] direction.

Plan-view bright-field and dark-field TEM images, together with corresponding selected-area electron diffraction (SAED) pattern, of the $Ti_{0.67}Hf_{0.33}B_{1.7}$ thin film are shown in Fig. 4. The bright-field and dark-field TEM images, Fig. 4(a) and (b), reveal that the $Ti_{0.67}Hf_{0.33}B_{1.7}$ layer has a fully-dense nanostructure with no discernible porosity. Individual crystalline columns exhibit non-uniform, speckled contrast that is an indication of strained, distorted lattice as a result of residual ion-irradiation induced damage. The SAED pattern in the inset of Fig. 4(a) indicates that the $Ti_{0.67}Hf_{0.33}B_{1.7}$ columns are highly oriented along the growth direction [0001], characterized by a dominant $10\bar{1}0$ signal in plan-view and missing $000l$ reflections, which is consistent with the XRD result in Fig. 3. While the densification effects demonstrated herein concerned films grown on sapphire substrates, we foresee the transferability to other substrates like for cutting tools as the governing process factor is the interaction of heavy-mass Hf^+ irradiation with the TiB_2 film.

To elucidate the mechanism of heavy-mass-ion-bombardment-induced densification, we carried out TRIM [27] simulations of 300-eV Hf ions impinging on $Ti_{0.67}Hf_{0.33}B_{1.7}$. The effect of lower-mass ion irradiation present during the 200-μs bias pulses (B^+ and Ar^+, see Fig. 1) is also simulated, but due to their lower ion fluxes involved, it is small and therefore not discussed further. Fig. 5 shows the depth distributions of subplanted Hf projectiles, along with those for Ti, Hf, and B recoils. The heavy Hf ions produce a significant number of low-energy lattice recoils; ~5.1 recoils are generated per incident ion, from which ~1.9 are B recoils, ~2.1 are Ti recoils, and ~1.1 are Hf recoils. Due to the large mass mismatch, the B recoils have lower energy and remain closer to the surface with the projected range plus straggle of ~1.5 nm, while the corresponding values for the Ti and Hf recoils are ~2.0 and

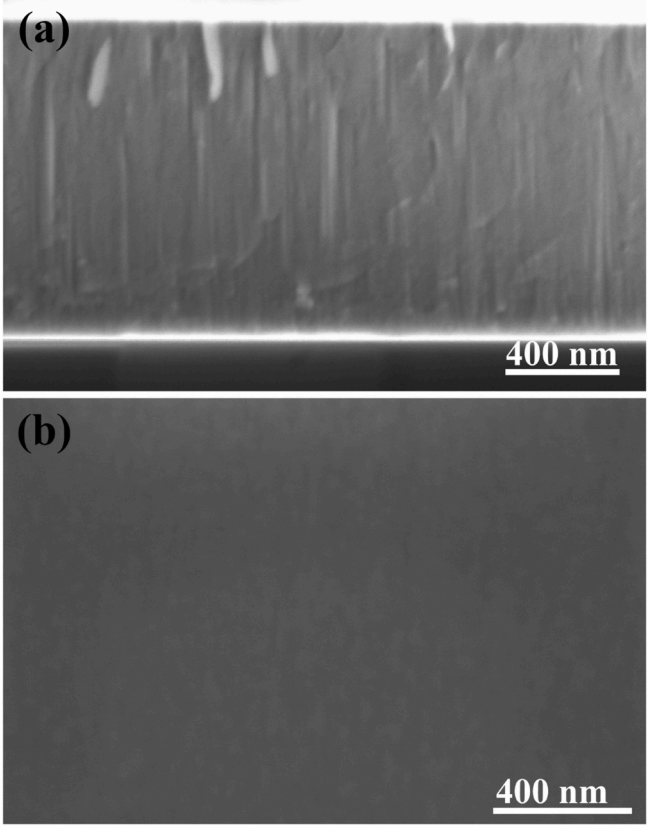

Fig. 2. Cross-sectional and plan-view SEM images of $Ti_{0.67}Hf_{0.33}B_{1.7}$ thin film grown without external heating at the substrate temperature lower than 100 °C.

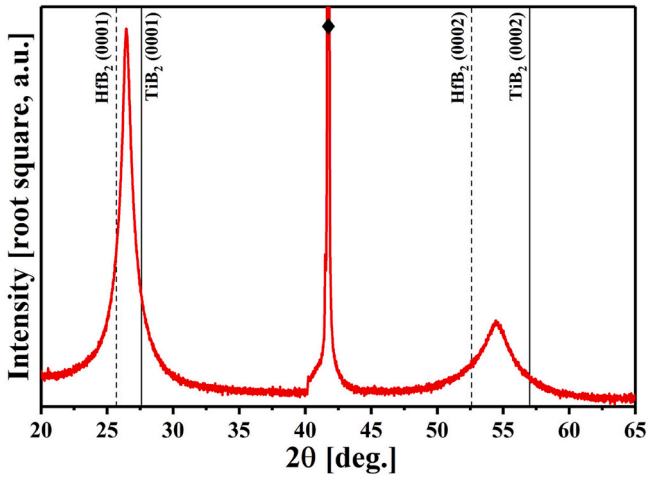

Fig. 3. The XRD θ-2θ scan of $Ti_{0.67}Hf_{0.33}B_{1.7}$ thin film grown without external heating at the substrate temperature lower than 100 °C.

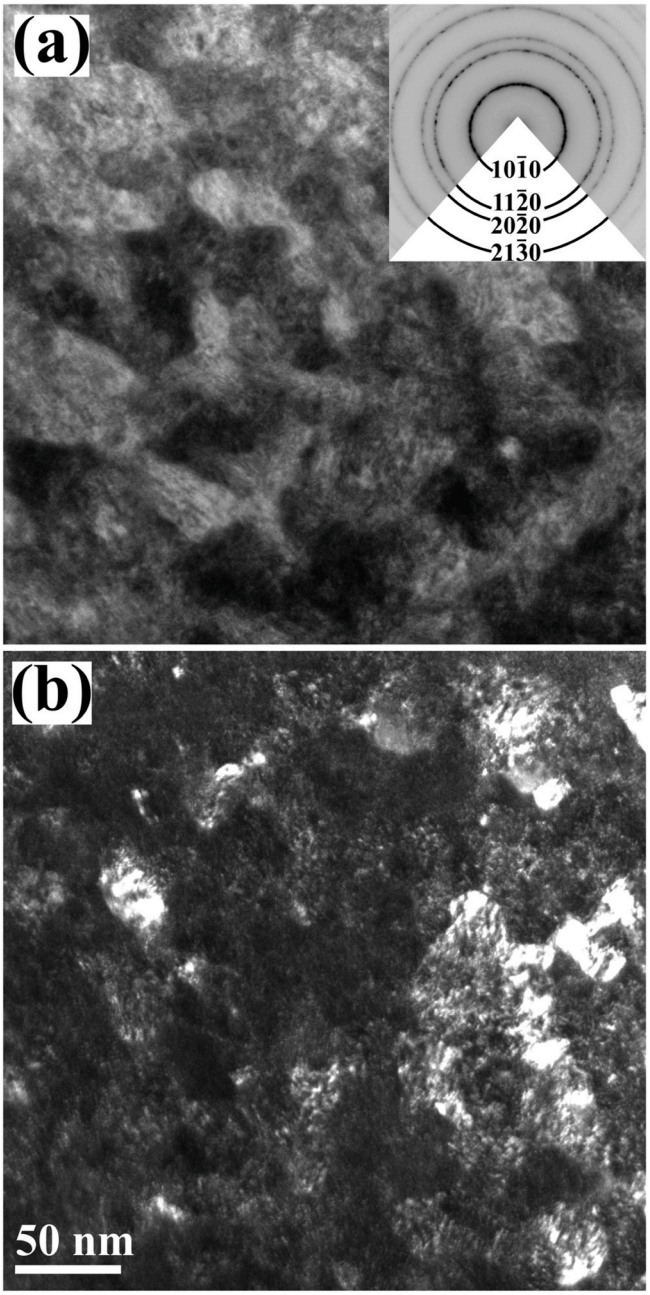

Fig. 4. Plan-view (a) bright-field, with corresponding SAED pattern in inset, and (b) dark-field TEM images of $Ti_{0.67}Hf_{0.33}B_{1.7}$ thin film grown without external heating at the substrate temperature lower than 100 °C.

~2.2 nm, respectively. Thus, the region of intense recoil mixing induced by the Hf ions can be divided into two sub-regions: (i) a sublayer with a thickness of below ~1.5 nm (region A in Fig. 5), in which all target atoms are displaced, and (ii) a sublayer with a thickness between ~1.5 nm and ~2.2 nm (region B in Fig. 5), in which the cation recoils (Ti and Hf) are dominant. In addition to different regions of the recoil generation, the energy transferred to the recoils is also strongly dependent on their masses. The maximum energy transfer in binary head-on collisions of Hf with target atoms (γ) can be calculated by

$$\gamma = 4m_{Hf}m_T / \left(m_{Hf} + m_T\right)^2, \quad (1)$$

where m_{Hf} and m_T are the masses of incident Hf ions and target atoms involved in the collision, respectively [28]. The γ value increases from 0.22 for B ($m_B = 10.8$ amu) to 0.67 for Ti ($m_{Ti} = 47.9$ amu) and 1 for Hf

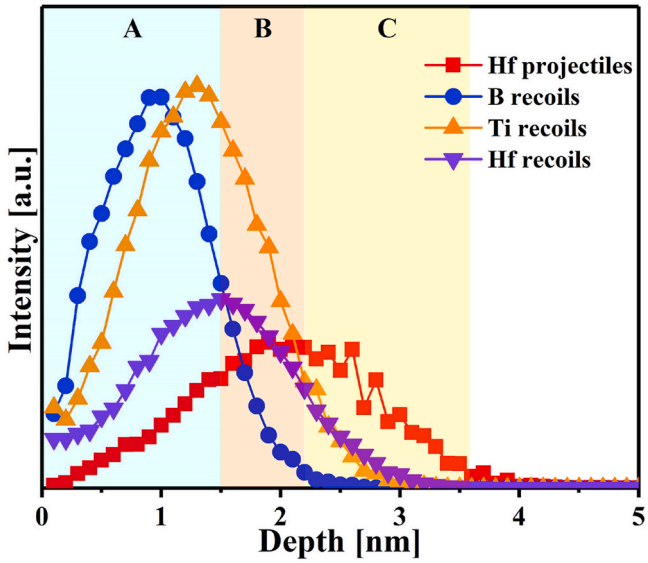

Fig. 5. Depth profiles of Hf projectiles together with Ti, Hf, and B recoils during hybrid HiPIMS/DCMS co-sputtering of $Ti_{0.67}Hf_{0.33}B_{1.7}$ obtained using TRIM2013 calculations.

($m_{Hf} = 178.5$ amu). Hence, the ion energy is predominantly transferred to the cation (Ti and Hf) sublattice. The B recoils receive 25% of the deposited energy, while the Ti and Hf recoils absorb 45% and 30% of the energy, respectively. The high-mass Hf projectiles, which scatter relatively little sideways, penetrate beyond the region of intense recoil mixing (regions A and B) and contribute to an additional densification of the films (region C in Fig. 5). As a result, the heavy Hf^+ ion irradiation leads to the film densification with intense ion mixing of the metal atoms.

The nanoindentation hardness H of the $Ti_{0.67}Hf_{0.33}B_{1.7}$ film is ~41.0 GPa and is ascribed to the dense nanostructure, solid-solution formation, and defect hardening. The latter results from the intense ion-irradiation-induced lattice damage with local distortions in atomic positions. The nanoindentation elastic modulus E is ~441.0 GPa, which is lower than the elastic modulus of bulk TiB_2 (~565 GPa [20]) and $Ti_{0.67}Hf_{0.33}B_2$ (~540 GPa, estimated from Vegard's law), due to a large number of ion-irradiation-induced defects as well as the lower-density column boundaries compared to the single-crystal sample.

4. Conclusions

We report the growth of dense $Ti_{0.67}Hf_{0.33}B_{1.7}$ thin films without external heating by hybrid HfB_2-HiPIMS/TiB_2-DCMS co-sputtering in pure Ar on $Al_2O_3(0001)$ substrates. Applying a substrate bias potential of −300 V during the target-ion-rich portion of each HiPIMS pulse results in a significant energy and momentum transfer to the growing film causing effective low-energy recoils generation. Hence, the decreased atomic mobility due to the low-temperature growth is compensated by heavy-mass ion irradiation that leads to the growth of a dense and smooth $Ti_{0.67}Hf_{0.33}B_{1.7}$ thin films with a hardness of ~41.0 GPa. These results prove that the novel thin film growth method previously demonstrated for reactively-sputtered transition metal (TM) nitrides, works also for TM diborides sputtered from compound targets. Hence, the prospects for significant energy saving by means of eliminating process heating requirements are not limited to one particular class of materials. Additional benefit is that the process envelope can be extended to cover film growth on temperature-sensitive substrates.

Declaration of competing interest

The authors declare that they have no known competing financial

interests or personal relationships that could have appeared to influence the work reported in this paper.

Acknowledgments

We acknowledge support from the Knut and Alice Wallenberg (KAW) foundation for Project funding (KAW 2015.0043), a Fellowship/Scholar Grant, and support of the electron microscopy laboratory in Linköping. Financial support from the Swedish Research Council VR Grant 2018-03957, and 642-2013-8020, the VINNOVA Grant 2019-04882, the Swedish Energy Agency grant 51201-1, and Carl Tryggers Stiftelse contracts CTS 15:219, CTS 17:166, and CTS 14:431 are also gratefully acknowledged. Furthermore, the authors acknowledge financial support from the Swedish Government Strategic Research Area in Materials Science on Functional Materials at Linköping University (Faculty Grant SFO Mat LiU No. 2009 00971). Supports from the Swedish research council VR-RFI (#2017-00646_9) for the Accelerator based ion-technological center and from the Swedish Foundation for Strategic Research (contract RIF14-0053; for the tandem accelerator laboratory in Uppsala University, and contract RIF14-0074; for the electron microscopy laboratory) are acknowledged. JMS most gratefully acknowledges funding from the German Science Foundation (DFG) within SCHN735/42-1.

References

[1] D.M. Mattox, G.J. Kominiak, Structure modification by ion bombardment during deposition, J. Vac. Sci. Technol., A 9 (1) (1972) 528–532.
[2] G. Håkansson, J.E. Sundgren, D. McIntyre, J.E. Greene, W.D. Münz, Microstructure and physical properties of polycrystalline metastable $Ti_{0.5}Al_{0.5}N$ alloys grown by d.c. magnetron sputter deposition, Thin Solid Films 153 (1) (1987) 55–65.
[3] I. Petrov, P.B. Barna, L. Hultman, J.E. Greene, Microstructural evolution during film growth, J. Vac. Sci. Technol., A 21 (5) (2003) S117–S128.
[4] T. Lee, H. Seo, H. Hwang, B. Howe, S. Kodambaka, J.E. Greene, I. Petrov, Fully strained low-temperature epitaxy of TiN/MgO(001) layers using high-flux, low-energy ion irradiation during reactive magnetron sputter deposition, Thin Solid Films 518 (18) (2010) 5169–5172.
[5] G. Greczynski, I. Petrov, J.E. Greene, L. Hultman, Paradigm shift in thin-film growth by magnetron sputtering: from gas-ion to metal-ion irradiation of the growing film, J. Vac. Sci. Technol., A 37 (6) (2019). Article 060801.
[6] G. Greczynski, J. Lu, S. Bolz, W. Kölker, C. Schiffers, O. Lemmer, I. Petrov, J. E. Greene, L. Hultman, Novel strategy for low-temperature, high-rate growth of dense, hard, and stress-free refractory ceramic thin films, J. Vac. Sci. Technol., A 32 (4) (2014), 041515.
[7] T.C. Huang, G. Lim, F. Parmigiani, E. Kay, Effect of ion bombardment during deposition on the x-ray microstructure of thin silver films, J. Vac. Sci. Technol., A 3 (6) (1985) 2161–2166.
[8] L. Hultman, J.E. Sundgren, L.C. Markert, J.E. Greene, Ar and excess N incorporation in epitaxial TiN films grown by reactive bias sputtering in mixed Ar/N_2 and pure N_2 discharges, J. Vac. Sci. Technol., A 7 (1989), 1187.
[9] A.K. Agarwal, A. Garg, D.K. Srivastava, M.K. Shukla, Comparative wear performance of titanium based coatings for automotive applications using exhaust gas recirculation, Surf. Coating. Technol. 201 (13) (2007) 6182–6188.
[10] J.C. Schuster, J. Bauer, The ternary system titanium-aluminum-nitrogen, J. Solid State Chem. 53 (2) (1984) 260–265.
[11] I. Petrov, F. Adibi, J.E. Greene, L. Hultman, J.E. Sundgren, Average energy deposited per atom: a universal parameter for describing ion-assisted film growth, Appl. Phys. Lett. 63 (1) (1993) 36–38.
[12] J. Bohlmark, J. Alami, C. Christou, A.P. Ehiasarian, U. Helmersson, Ionization of sputtered metals in high power pulsed magnetron sputtering, J. Vac. Sci. Technol., A 23 (2005) 18–22.
[13] S.M. Rossnagel, Gas density reduction effects in magnetrons, J. Vac. Sci. Technol., A 6 (1) (1988) 19–24.
[14] D.W. Hoffman, A sputtering wind, J. Vac. Sci. Technol., A 3 (3) (1985) 561–566.
[15] G. Greczynski, J. Lu, J. Jensen, I. Petrov, J.E. Greene, S. Bolz, W. Kölker, C. Schiffers, O. Lemmer, L. Hultman, Metal versus rare-gas ion irradiation during $Ti_{1-x}Al_xN$ film growth by hybrid high power pulsed magnetron/dc magnetron co-sputtering using synchronized pulsed substrate bias, J. Vac. Sci. Technol., A 30 (6) (2012), 061504.
[16] Z. Wu, O. Tengstrand, B. Bakhit, J. Lu, J.E. Greene, L. Hultman, I. Petrov, G. Greczynski, Growth of dense, hard yet low-stress $Ti_{0.40}Al_{0.27}W_{0.33}N$ nanocomposite films with rotating substrate and no external substrate heating, J. Vac. Sci. Technol., A 38 (2) (2020), 023006.
[17] H. Fager, O. Tengstrand, J. Lu, S. Bolz, B. Mesic, W. Kölker, C. Schiffers, O. Lemmer, J.E. Greene, L. Hultman, I. Petrov, G. Greczynski, Low-temperature growth of dense and hard $Ti_{0.41}Al_{0.51}Ta_{0.08}N$ films via hybrid HIPIMS/DC magnetron co-sputtering with synchronized metal-ion irradiation, J. Appl. Phys. 121 (17) (2017), 171902.
[18] G. Greczynski, L. Hultman, Time and energy resolved ion mass spectroscopy studies of the ion flux during high power pulsed magnetron sputtering of Cr in Ar and Ar/N_2 atmospheres, Vacuum 84 (9) (2010) 1159–1170.
[19] W.C. Oliver, G.M. Pharr, An improved technique for determining hardness and elastic modulus using load and displacement sensing indentation experiments, J. Mater. Res. 7 (6) (1992) 1564–1583.
[20] R.G. Munro, Material properties of titanium diboride, J. Res. Natl. Inst. Stand Technol. 105 (5) (2000) 709–720.
[21] H. Liang, W. Sun, X. Li, H. Chen, S. Guan, P. Liu, Q. Wang, X. Li, D. He, F. Peng, Study of the compression behavior and elastic properties of HfB_2 ceramics using experimental method and first-principles calculations, J. Alloys Compd. 808 (2019), 151764.
[22] G. Greczynski, I. Zhirkov, I. Petrov, J.E. Greene, J. Rosen, Time evolution of ion fluxes incident at the substrate plane during reactive high-power impulse magnetron sputtering of groups IVb and VIb transition metals in Ar/N_2, J. Vac. Sci. Technol., A 36 (2018), 020602.
[23] G. Greczynski, I. Petrov, J.E. Greene, L. Hultman, Strategy for tuning the average charge state of metal ions incident at the growing film during HIPIMS deposition, Vacuum 116 (2015) 36–41.
[24] D.R. Lide, CRC Handbook of Chemistry and Physics, Section 10, Atomic, Molecular, and Optical Physics; Ionization Potentials of Atoms and Atomic Ions, CRC, Boca Raton, FL, 2003.
[25] JCPDS International Centre for Diffraction Data, Titanium Diboride (TiB_2) Card00-035-0741.
[26] JCPDS International Centre for Diffraction Data, Hafnium Diboride (HfB_2) Card00-012-0234.
[27] J.F. Ziegler, M.D. Ziegler, J.P. Biersack, Srim - the stopping and range of ions in matter (2010), Nucl. Instrum. Methods B 268 (11) (2010) 1818–1823.
[28] M. Nastasi, J.W. Mayer, Y. Wang, Ion Beam Analysis: Fundamentals and Applications, CRC, Taylor & Francis group, Boca Raton, FL, 2014.